

# Testing and parametric modeling of magnetorheological valve with meandering flow path

Fitrian Imaduddin · Saiful Amri Mazlan ·  
Ubaidillah · Hairi Zamzuri ·  
Abdul Yasser Abd Fatah

Received: 10 March 2015 / Accepted: 13 February 2016 / Published online: 9 March 2016  
© Springer Science+Business Media Dordrecht 2016

**Abstract** The experimental testing and a new hysteresis modeling approach of a magnetorheological (MR) valve with meandering flow path formed by combination of multiple annular and radial gaps are presented. The dynamic behavior of the valve is evaluated using a dynamic test machine in displacement control mode based on the relationship between the valve pressure drop, the fluid flow rate and the magnitude of input current to the electromagnetic coil. In order to model the hysteresis behavior of the MR valve, a new parametric modeling approach is proposed based on the LuGre friction operator with some modifications to reduce the number of parameters involved. The parameters for each testing data are then identified using gradient descent method, and the parameter distribution is then approximated with polynomial functions. According to the performance assessment results, it can be concluded that the LuGre-based parametric hystere-

sis model is able to follow the hysteresis behavior of the MR valve within a particular range of excitation frequencies.

**Keywords** Magnetorheological valve · Dynamic testing · Parametric modeling · Hysteresis

## 1 Introduction

Magnetorheological (MR) dampers have been integrated with control system in many applications such as in automotive semi-active suspension systems [1–5] and in seismic vibration control in various civil structures [6–10]. The integration process between MR dampers and controllers normally requires a set of mathematical model [11]. In terms of modeling purpose, the MR damper model can be divided into two types, the inverse dynamic model and the forward dynamic model [12]. The inverse dynamic MR damper model is commonly used as a part of the controller since the model can be used to predict the desired current input to achieve a specific damping force in a particular rod velocity [13–16]. Meanwhile, the forward MR damper model is commonly used in the design stage of the controller as the virtual representation of the physical MR damper [17].

As a virtual representation of the physical MR damper, the behavior of the MR dampers in the forward model can be described in two ways, the steady-state behavior and dynamic behavior. The steady-state

---

F. Imaduddin (✉) · H. Zamzuri · A. Y. A. Fatah  
Vehicle System Engineering Research Laboratory,  
Universiti Teknologi Malaysia, Jalan Sultan Yahya Petra,  
54100 Kuala Lumpur, Malaysia  
e-mail: ifitrian2@live.utm.my

S. A. Mazlan  
Malaysia-Japan International Institute of Technology,  
Universiti Teknologi Malaysia, Jalan Sultan Yahya Petra,  
54100 Kuala Lumpur, Malaysia  
e-mail: amri.kl@utm.my

Ubaidillah  
Mechanical Engineering Department, Faculty of Engineering,  
Universitas Sebelas Maret, Jalan Ir. Sutami 36A, Kentingan,  
Surakarta 57126, Indonesia

behavior of the MR damper is commonly defined as a linear damper behavior when no variation in variables is involved. The dynamic behavior, on the other hand, is normally defined as a nonlinear damper behavior when the influenced variables are changing over time. According to Snyder et al. [18], the linear steady-state behavior model is only sufficient to predict the energy dissipation; however, it cannot accurately portrays the force response of the MR damper. The force response of an MR damper is known as a highly nonlinear variable that depends on the amplitude and frequency of motion and can only be modeled using nonlinear dynamic model [19,20].

Many methods have been proposed to model the dynamic behavior of MR damper. In general, the modeling approaches of MR damper can be divided into two types, the parametric modeling and nonparametric modeling. Parametric modeling is the approach that utilizes a collection of mechanical elements as a hypothetical representation of the device so that the behavior can be mathematically modeled using the dynamic relationship between these elements. There are various kinds of parametric model that have been developed [20–33]. One of the most known parametric models is the Bouc–Wen model that has been widely used to model the MR damper [20,23,25–27]. Nonparametric modeling, on the other hand, is approaching the modeling problem with analytical expression to describe the device characteristics based on the testing data [31]. There are various methods that have been executed to model the MR damper behavior with nonparametric approach such as the neural network [17,34–37], and the polynomial model [2,38,39].

Parametric approach has the advantages due to its ability to provide a generalized form of the model, which means that the same form can be used repeatedly in other devices. Nevertheless, there are pitfalls in the accuracy of the results since the model ability to follow the device behavior is limited and in order to mimic the characteristics of a specific device in a good match, the involvement of a rigorous parameter identification method is mandatory [26,27]. On the contrary, the nonparametric approach is able to avoid the problem in modeling accuracy; however, there is no generalized form since the model form will be unique for each device and the development is highly dependent on a specific testing data. Hence, the process flow to generate the nonparametric model is typically more complicated than the parametric model and the valid-

ity of the generated model is only limited to a specific device that is incorporated in the modeling process.

While the modeling approaches for MR damper have been widely discussed, the dynamic modeling technique, particularly the parametric model, of MR valve as a single component is rarely disseminated. The current literatures that discussed the MR valve design and modeling mostly presented only the steady-state model of the valve due to the focus limitation in predicting the valve peak performance [40–45]. However, in terms of control design purpose, the steady-state model only will not adequately represent the device behavior. The necessity of dynamic modeling of MR valve also can be considered higher than MR damper because the MR valve and the model can be used in wider range of applications aside of MR damper. For example, the knowledge of MR valve behavior and its virtual representation can be used as a reference to design and predict the performance of an MR damper [46] or to help further development of new concept of actuators that require MR fluid flow control [47,48].

Considering the importance of MR valve in the advancement of MR fluid applications, this paper intends to elaborate the dynamic behavior of MR valve as a single component. The MR valve that is specifically discussed in this study is the high-performance MR valve with meandering flow path proposed by Imaduddin et al. [44]. The valve has shown the ability to generate pressure drop more than 6 MPa in a relatively similar dimension and power consumption with its predecessors that only generate around 2.5 MPa. The specific objective of this paper is to present the dynamic testing of the MR valve with meandering flow path as a single component and its dynamic modeling using a new parametric modeling approach. The dynamic testing of the MR valve is conducted using a dynamic test machine, and the results are expressed in the relationship between valve pressure drop and fluid flow rate at various current excitations to the electromagnetic coil of the valve. The new parametric model for MR valve adapts the LuGre hysteretic model as its base form with modifications to reduce the number of parameters involved. In order to fit the model output with the testing data, the gradient descent method is used to estimate the parameter values. The estimated parameters are then approximated with polynomial functions to complete the specific form of the parametric model.

The paper is organized as follows: the experimental setup of the dynamic testing is presented in Sect. 2 and

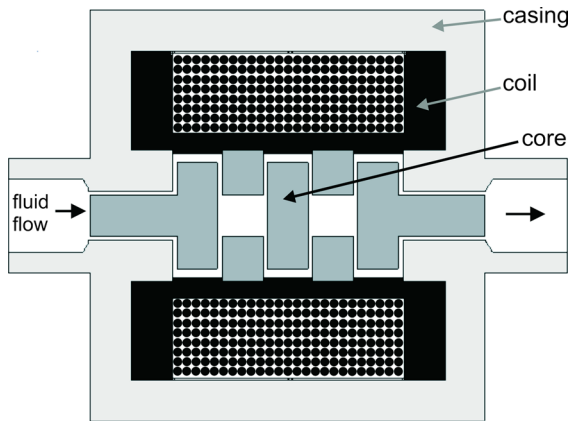


**Fig. 1** MR valve with meandering flow path [44]

the experimental results of the MR valve is explained in Sect. 3, while the parametric modeling procedures of the MR valve are discussed in Sect. 4. The evaluations of the model performance are elaborated in Sect. 5, and finally, the conclusion of the paper is summarized in the end of the paper.

## 2 Experimental testing

### 2.1 Experimental apparatus

The MR valve discussed in this paper is the new class of MR valve based on the concept that was proposed by Imaduddin et al. [44] as shown in Fig. 1. The concept has introduced the combination of several annular and radial channels in the MR valve to form a meandering flow path in order to expand the effective magnetization area. The improvement of valve pressure drop has been predicted with the meandering flow path approach [49]. The experimental work also has been conducted and shown that the steady-state behavior of the valve generally matches with the prediction [44]. However, since the derived steady-state model cannot reveal the dynamic behavior of the MR valve, the measurement will be used to observe the dynamics.

The MR valve structure is mainly divided into three components, which are the casing, the coil and the valve core. The casing is made from AISI 1010 compatible mild steel and consists of two identical parts, which each of them also has a fluid channel with female BSPP 1/4" port and four holes for locking bolts. The coil

**Table 1** Typical properties and material compatibility of MRF-132DG [50,55]

Fluid properties	
Base fluid	Hydrocarbon
Solid content by weight (%)	80.98
Density (g/cm <sup>3</sup> ) [lb/gal]	2.95–3.15 (24.6–26.3)
Operating temperature [°C (°F)]	–40 to 130 (–40 to 266)
Flash point [°C (°F)]	>150 (>302)
Viscosity, Pa·s @ 40°C (104°F)	0.092 ± 0.015
Calculated as slope 800–1200 s <sup>–1</sup>	
Material compatibilities	
Buna N (Nitrile)	Good
Butyl	Poor
EPDM/EPR	Poor
Fluoroelastomer	Good
Natural rubber	Poor
Neoprene	Good
Silicone	Fair
Iron	Good
Stainless steel	Good
Aluminum	Good
Polyurethane	Good

consists of copper wire windings and an aluminum coil bobbin, which has a groove on each side for O-ring installation as a sealing mechanism. The coil bobbin also has four M2 threaded holes in each side as a bolt-locking mechanism with the casing. The specific MR fluid that is used in this study is the MRF-132DG, an MR fluid made by Lord Corporation for general use in controllable, energy-dissipating applications such as shocks, dampers and brakes [50–52]. Viton is selected as the O-ring material rather than rubber due to poor compatibility of rubber with hydrocarbon as the carrier liquid of the MRF-132DG (see Table 1). The selection of Viton is also referred to several references [53,54], which utilized the same material for their sealing for hydrocarbon based MR fluid. The last component is the valve core which consists of several parts, namely two mild steel side cores, two mild steel orifice cores, a mild steel center core and six aluminum spacers. The spacers are used to maintain the clearance between core parts. The exploded view of the MR valve design is shown in Fig. 2.

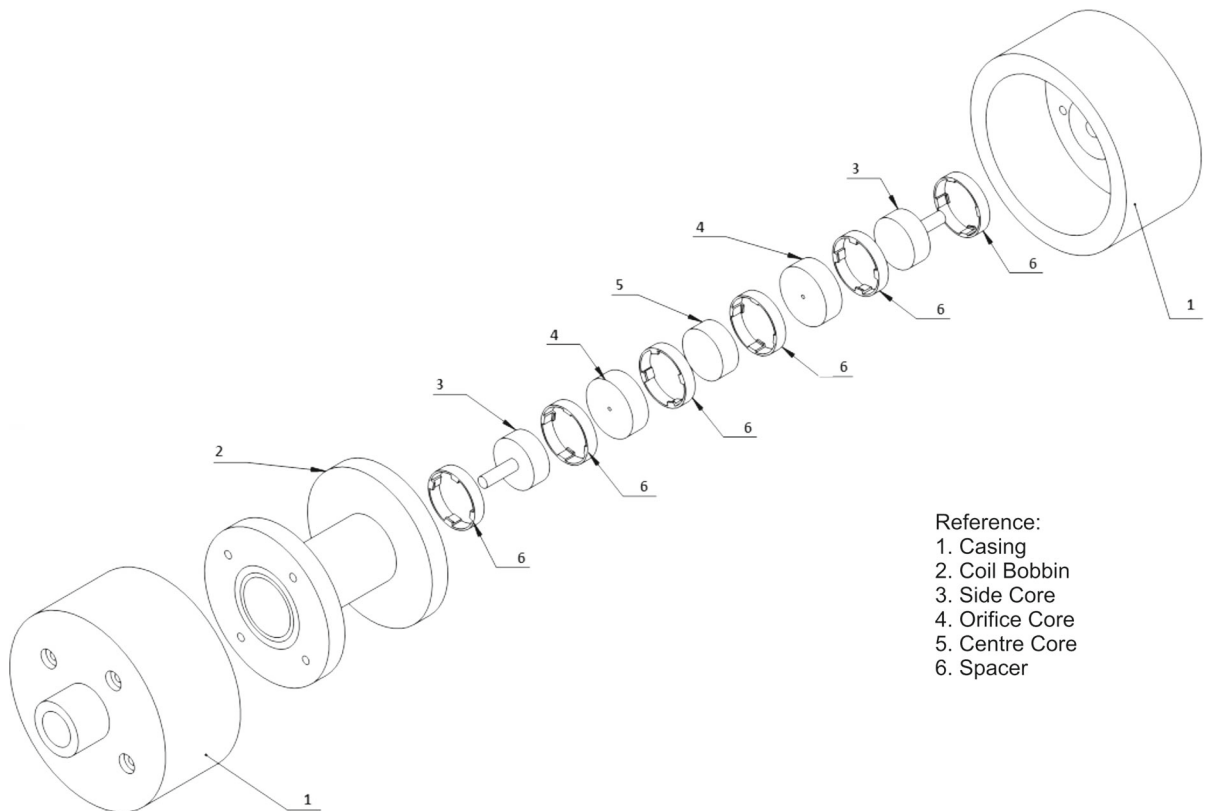


**Fig. 2** Exploded view of the MR valve prototype

In order to observe the dynamic behavior of MR valve, the flow of MR fluid needs to be induced across the valve. There are various methods that have been used by researchers to induce flow of MR fluid such as demonstrated in [56–58]. The method that is chosen to induce fluid flow in this study is similar to the method used in [40], where the MR valve is installed in the bypass channel of a hydraulic cylinder, which is fully filled with MR fluid. The fluid flow was then induced by introducing movement to the hydraulic cylinder, which act as the MR valve testing cell, using dynamic test machine. In this study, the MR valve with meandering flow path that is tested has 0.5 mm radial gap and 0.5 mm annular gap that was reported to have achievable pressure drop over 6 MPa [44]. Meanwhile, the testing cell that is used to test the MR valve is made from a double-rod hydraulic cylinder with fully sealed piston. The sealed piston is needed to ensure that the passage to flow across chambers is only through the bypass channel that has been obstructed by the MR valve. The bore size of the cylinder is 30 mm with maximum stroke length and diameter of the rod are

70 mm and 18 mm, respectively (the net piston area is around  $452.4 \text{ mm}^2$ ). The double-rod cylinder is used as the testing cell to eliminate the requirement of accumulator since no volume compensation is needed during operation. The prototype of MR valve with meandering flow path is installed in the testing cell as shown in Fig. 3.

## 2.2 Experimental arrangement

The experimental arrangements to observe the dynamic behavior of the MR valve are described as follows: MR valve prototype is installed in a testing cell made from a double-rod hydraulic cylinder with a bypass configuration (see Fig. 3). To actuate the testing cell, a stroke-controlled sinusoidal wave is generated using the Shimadzu Dynamic Test Machine as shown in Fig. 4. The machine is equipped with a 20 kN force sensor and a displacement sensor. The sinusoidal actuation to the testing cell will generate an alternating pressure-induced flow to the MR valve every time the rod is compressed and extended by the dynamic machine.



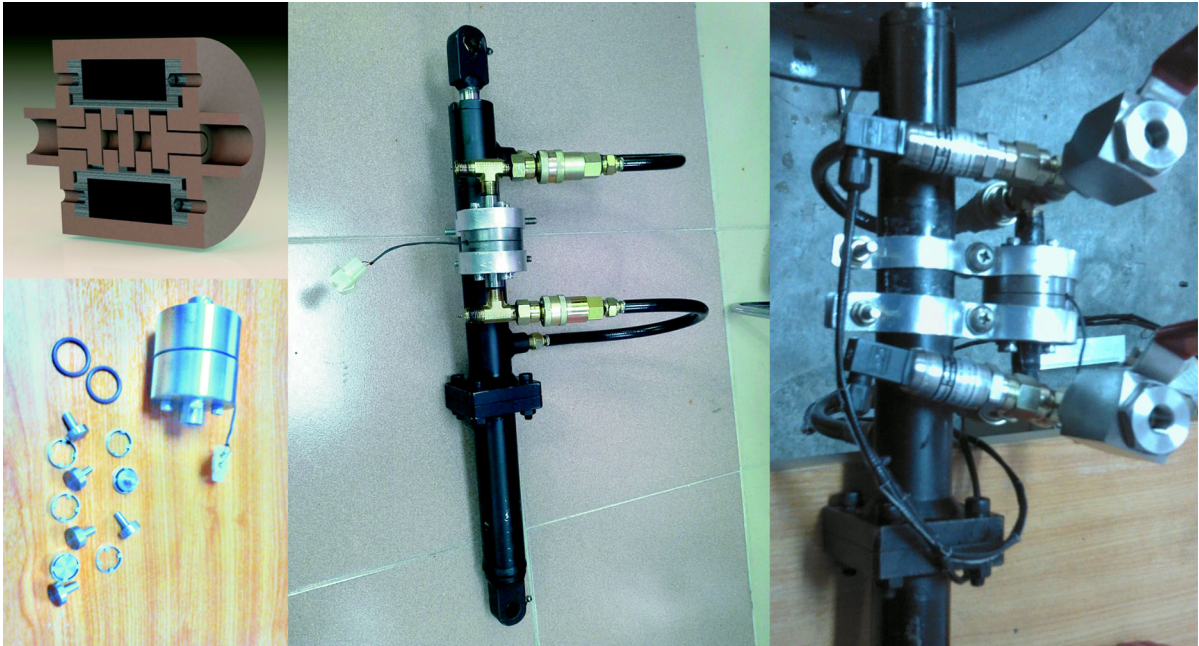


**Fig. 3** MR valve installation in the testing cell

For instance, the arrangement of the MR valve in the testing cell is similar to a bypass damper. However, as an MR valve testing cell, two pressure sensors are added to the bypass channel to directly measure the pressure drop of the MR valve. The installation point of the pressure sensors was selected in the nearest point to both MR valve ports to minimize the effect of additional pressure drop from the flow conduits.

In order to generate the flow, the testing cell is installed to the dynamic test machine where the cell is actuated in sinusoidal motion. The movement of the testing cell induces pressure difference between chambers of the cylinder and therefore generates flow across the MR valve. The measurement of velocity data is indirectly obtained by differentiating the displacement data from the displacement sensor of the dynamic test machine. Since the sinusoidal wave displacement can be expressed in  $u = A \sin(2\pi ft)$ , where  $A$  is the excitation amplitude of the displacement and  $f$  the frequency of excitation, the velocity of the rod is expressed in  $\dot{u} = -A2\pi f \cos(2\pi ft)$ . Using the velocity expression, the flow rate of the MR fluid can be expressed as:

$$Q = -\left(\pi \frac{D_{\text{cyl}}^2 - D_{\text{rod}}^2}{4}\right) A2\pi f \cos(2\pi ft) \quad (1)$$

where the  $D_{\text{cyl}}$  and  $D_{\text{rod}}$  are the bore diameter of the hydraulic cylinder and the rod diameter, respectively. As shown in Eq. (1), the flow rate of the MR fluid is only influenced by the dimensional parameters of the cylinder, the stroke length of excitation and the excitation frequency. Meanwhile, the variations in current input to the coil inside the valve are needed to adjust the magnetic field strength. The changing in the magnetic field strength will be used to demonstrate the MR effect through the proportional changing of the valve pressure drop. The summary of variable arrangement for the experimental test is given in Table 2.

### 3 Experimental results

#### 3.1 Effect of excitation frequency variation

The relationship between valve pressure drop against flow rate of the MR fluid at the coil current of 1.0 A at various frequencies is shown in Fig. 5. The results are the typical characteristics from the fifth cycle onwards since the characteristics of the first until the fourth cycle are usually unstable and inconsistent as similarly reported by Li et al. [59]. From Fig. 5, it can be concluded that the peaks of the valve pressure drop

**Fig. 4** MR valve testing cell installation in the testing machine

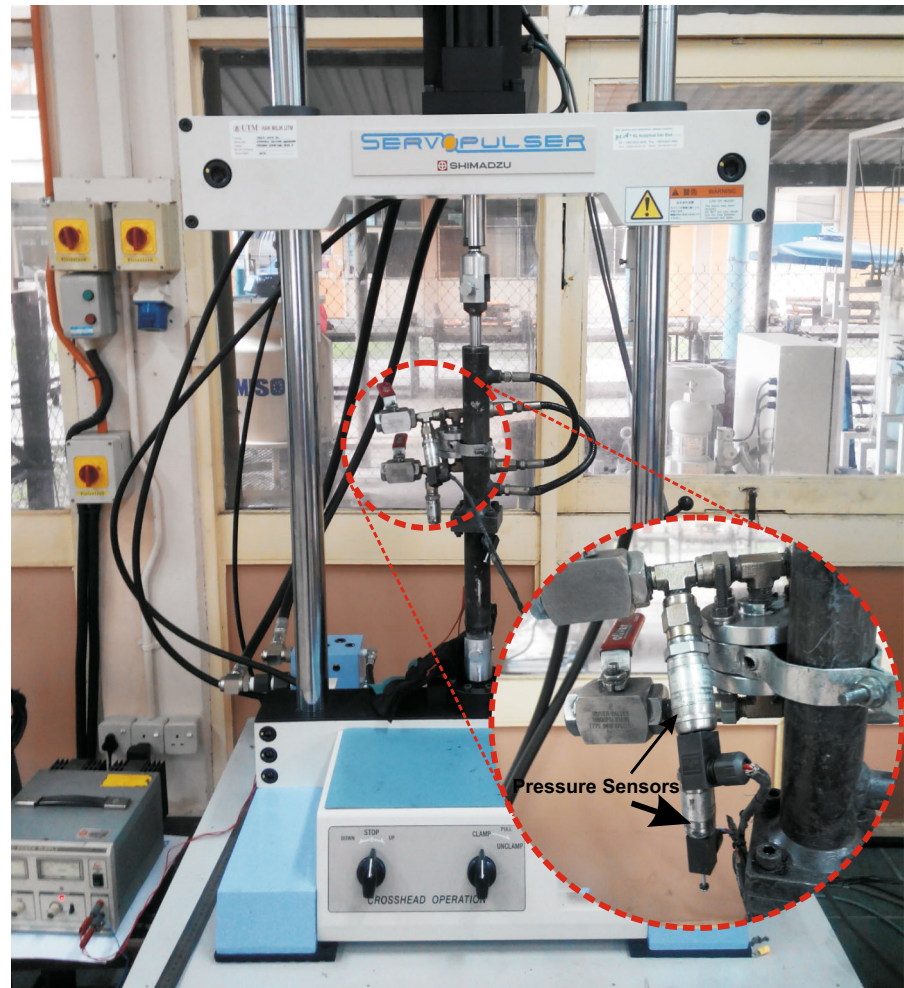


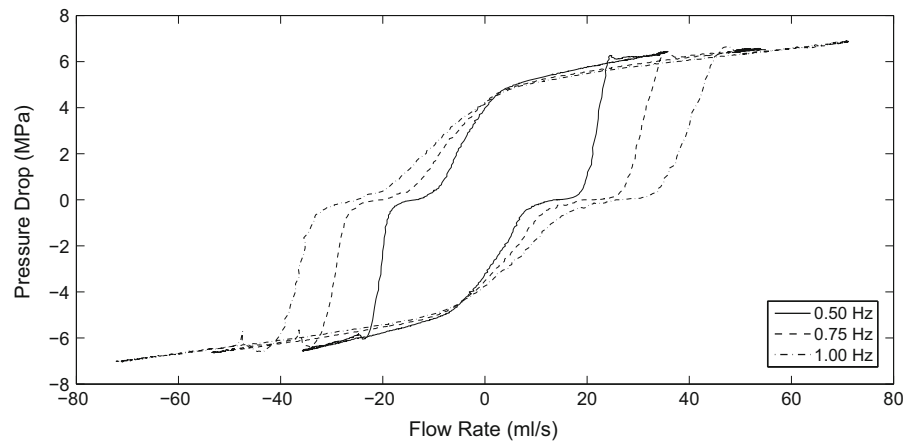
**Table 2** Variable arrangement of experimental test using Shimadzu Fatigue Dynamic Test Machine

Excitation frequency (Hz)	Excitation amplitude (mm)	Current input (A)	Cycles
0.50		0–1	
0.75	±25	(Interval 0.1)	25
1.00			

are increased with the increase in maximum flow rate. Similarly, the shifting of peak pressure drop also shifts the width of the hysteretic region. In other words, the width of the hysteretic region of pressure drop is highly dependent on the value of peak flow rate as typically found in the characteristics of MR damper in its analogous force-velocity pattern.

There is an interesting note regarding the bend of the curve shape in each time it passes through the 0 MPa of pressure drop. The bends of the curve were interpreted as the pressure lag effect similarly with the ones reported in the behavior of MR dampers by Yang [60] and Zhang et al. [61] which caused by the uncompressed air pocket that inevitably exists in the testing cell. The existence of air pocket inside the cylinder has created force lag effect to the characteristic curve. The force lag effect is occurred slightly after the pre-yield stress of the fluid reached zero. At this point, the air pocket is gradually compressed until the pressure is high enough to cause the flow of MR fluid. Such effect can be minimized by using vacuum technique in the fluid filling process as well as the utilization of the accumulator to pre-compress the air pocket in the damper assembly [60,62].

**Fig. 5** Pressure dynamics of MR valve at current input of 1 A at various frequency excitation



These effects apparently were not a unique case in the MR fluids device since its appearance was also reported in the characteristics of a passive hydraulic damper [63]. Since no report has strongly mentioned about side effects of the air pocket to the overall damping characteristics other than just the force lag, in this study, the pressure lag effect will not be taken into consideration.

### 3.2 Effect of current input variation

Figure 6a–c shows the characteristics of valve with current input variations at 0.50, 0.75 and 1.00 Hz of excitation frequencies. As predicted, the MR valve with meandering flow path is consistently showing pressure drop adjustment with the variation in the current input. As seen in Fig. 6a, the peak pressure drop is around 0.65 MPa at the current of 0.0 A with 0.50 Hz excitation frequency. When the current increases in the interval of 0.1 A, the peak pressure drop is also steadily increased with average increments of 0.58 MPa up to the maximum pressure drop of around 6.42 MPa at the current of 1.0 A. Similarly, in Fig. 6b, at the current of 0.0 A with 0.75 Hz excitation frequency the maximum pressure drop that can be achieved is around 0.95 MPa. However, with 0.1 A of current increment, the pressure drop are normally increased in around 0.56 MPa until the maximum observed pressure drop of 6.53 MPa is achieved at 1.0 A current. Lastly, at 1.00 Hz excitation frequency as shown in Fig. 6c, the maximum off-state pressure drop is around 1.35 MPa with the average increments of pressure drop being seen around 0.55 MPa with each 0.1 A increment of current so that the peak pressure drop at 1.0 A is measured at 6.86 MPa.

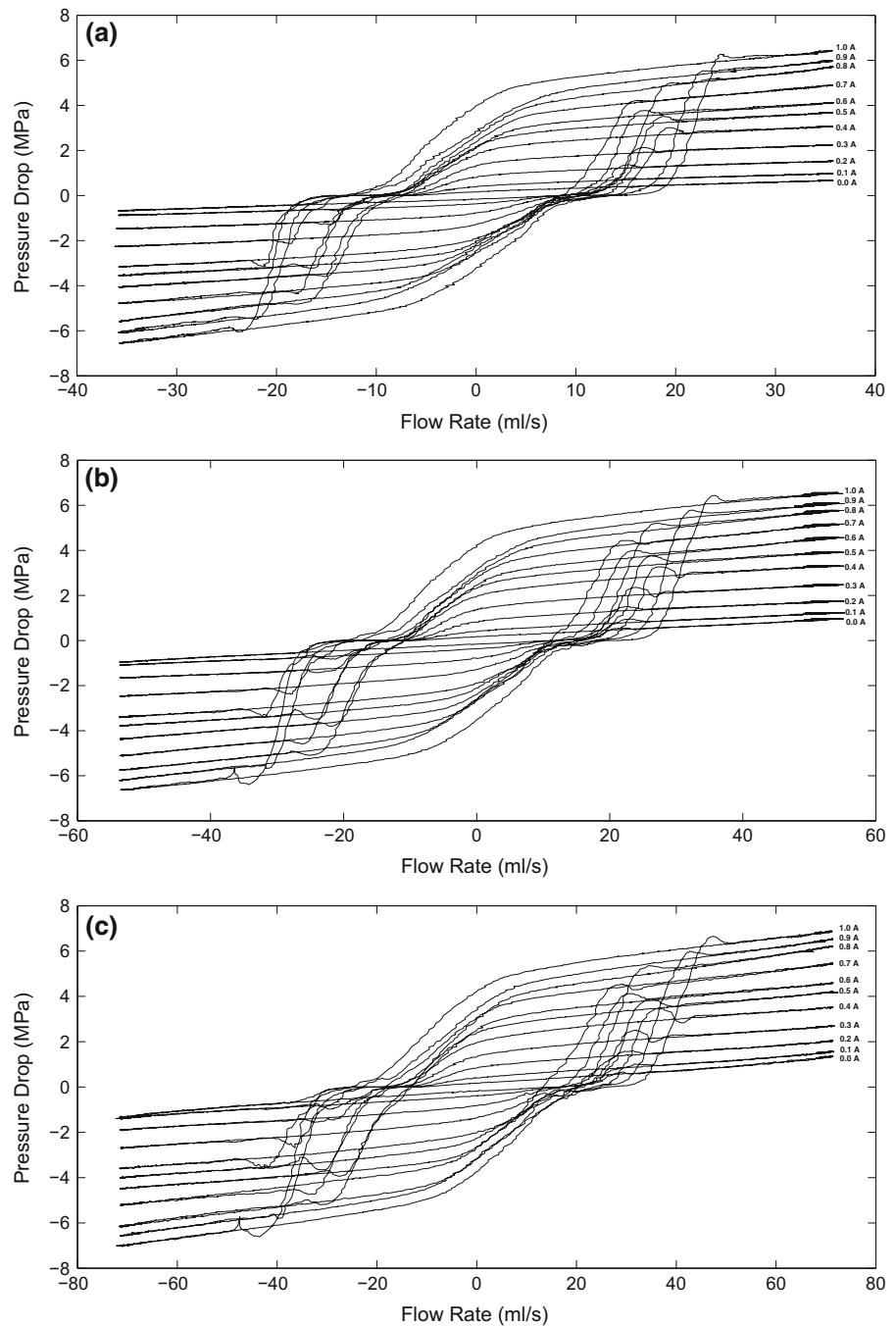
The relationships between peak pressure drop in each current increment for 0.50, 0.75 and 1.00 Hz excitation frequency are shown in Fig. 7.

As shown in Fig. 7, the rise of peak pressure drop is almost linear to the increment of the current input. However, there is an interesting phenomenon that can be observed from the curves where the slopes between 0.0 to 0.2 A and 0.8 to 1.0 A are slightly lower than those in the other regions. The phenomenon can be explained using the curve of yield stress versus magnetic field strength of the MRF-132DG, where the slope is linear at the lower magnetic field strength value and also leaner when it almost reached saturation in the higher magnetic field strength value. The declaration that the 1.0 A current input is already reached saturation region would be too premature, since according to the magnetic simulation demonstrated by Imaduddin et al. [44], the peak magnetic flux density at 1.0 A current input is only around 0.85 Tesla. The saturation region of the yield stress is started to visibly appear above 0.9 Tesla. However, the slope of the yield stress curve is already seen to gradually decrease after the magnetic flux density reached 0.7 Tesla. In the other words, it is assumed valid to predict that the attempt to increase the current input above 1.0 A will not give any significant improvement to the pressure drop performance of the MR valve, due to the yield stress saturation of the MR fluid.

## 4 Parametric model development

A parametric model is normally derived based on the mechanical idealization of a device. That is why most of the parametric models of an MR damper such as Bouc–

**Fig. 6** Pressure dynamics of MR valve at various current input, **a** 0.50 Hz, **b** 0.75 Hz, **c** 1.00 Hz

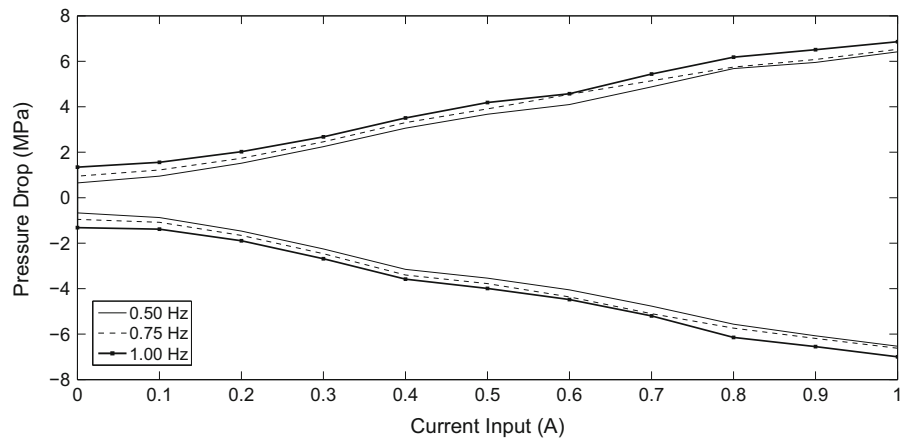


Wen model and Dahl model are represented by some sets of springs and dampers. Although there are also some other types of parametric models that are derived based on the nature of the curve shape of the experimental data such as the sigmoid function based models. There are normally two main issues that are considered

when a parametric model is derived. The first issue is regarding the model accuracy, and the second issue is about the number of parameters that should be identified. There are trade-offs regarding these issues, since the more accurate models often require more parameters to be identified. However, higher number of para-



**Fig. 7** Trend of peak pressure drop at various current input (0.50, 0.75 and 1.00 Hz produce peak flow rate of 35.53, 53.30 and 71.06 ml/s, respectively)



meters means higher computational cost due to the difficulties in the parameter optimization.

In order to model the hysteretic behavior of the MR valve with parametric modeling approach, the LuGre hysteresis model is used as a base. The LuGre model is the hysteretic model that initially developed to model the friction dynamics [64, 65] and is selected as the base model for the MR valve. The selection of LuGre model as the base model is mainly because hypothetically the flow dynamics is easier to be represented as friction dynamics rather than as a set of springs and dampers. The primary form of LuGre hysteresis model for MR damper is as follows:

$$F(t) = \sigma_0 z + \sigma_1 \dot{z} + \sigma_2 \dot{x} \tag{2}$$

where the  $\sigma_0$ ,  $\sigma_1$  and  $\sigma_2$  are the parameters of the model and  $z$  is the variable that can be expressed as:

$$\dot{z} = \dot{x} - \frac{|\dot{x}|}{g(\dot{x})} z \tag{3}$$

where  $g(\dot{x})$  is the additional function that depends on various factors such as material properties and temperature.

Further implementations of the LuGre model have brought some modifications to the primary form such as the modification proposed by Sakai et al. [21] that expressed the LuGre model as:

$$F(t) = \sigma_a z + \sigma_0 z v + \sigma_1 \dot{z} + \sigma_2 \dot{x} + \sigma_b \dot{x} v \tag{4}$$

$$\dot{z} = \dot{x} - \sigma_0 a_0 |\dot{x}| z \tag{5}$$

where  $\sigma_a$ ,  $\sigma_0$ ,  $\sigma_1$ ,  $\sigma_2$ ,  $\sigma_b$ , and  $a_0$  are the parameters of the model while  $v$  is the voltage input to the coil and the  $z$  is the evolutionary variable interpreted as the variable that models the pre-yield stiffness expressed as

the average MR fluid transient deformation generated when the direction of force is changing [66, 67].

The other modification to the LuGre model was also proposed by Jiménez and Álvarez-Icaza [22] in the following form:

$$F(t) = \sigma_{0b} z v + \sigma_1 \dot{z} + \sigma_{2a} \dot{x} \tag{6}$$

$$\dot{z} = \dot{x} - \sigma_{0b} \alpha a_0 |\dot{x}| z (1 + a_1 v) \tag{7}$$

where  $\sigma_{0b}$ ,  $\sigma_1$ ,  $\sigma_{2a}$ ,  $\alpha$ ,  $a_0$  and  $a_1$  are the parameters of the model, while  $v$  is similarly the applied voltage to the coil as well as the  $z$  as the evolutionary variable.

It can be seen that both forms use the voltage,  $v$ , as the input variable that is related to the coil magnetization strength. In another model, the magnetization strength is expressed with the magnitude of the current,  $i$ , given to the coil [20]. Physically both can be considered as equal term given that the change in coil resistance during magnetization is neglected. However, both current and voltage are just the indirect variables to express the units of magnetization strength. In other words, the value of voltage or current that is expressed in the model will not be universally applicable since the strength of magnetic field that influences the MR effect is also highly subjected to coil turns and dimensions.

Due to some differences between the modeling requirement of MR damper and MR valve, some modifications to the base form of the LuGre hysteresis model are needed to transform the form of forward damper model to the form of forward valve model as shown in Fig. 8. Some modifications of the base model are also made to reduce the number of parameters and simplify the model. Therefore, the generalized form of the modified LuGre-based MR valve model proposed in this paper is as follows:

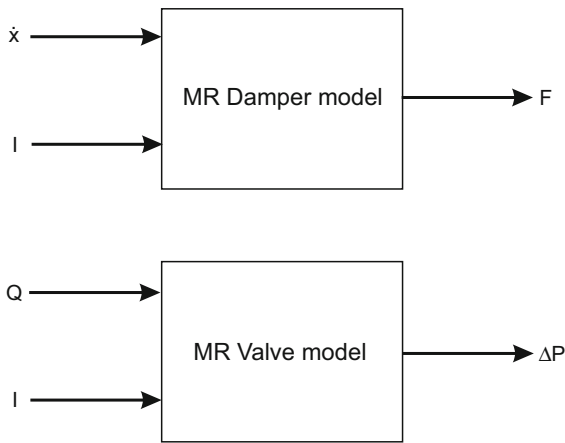


**Fig. 8** Difference between forward MR damper model and forward MR valve model excitation

$$\Delta P = Az + Bz + CQ^\alpha \tag{8}$$

$$\dot{z} = Q - a_0 |Q| z \tag{9}$$

Thus, there are five independent parameters that need to be identified, and these set of parameters are defined as follows:

$$\Theta = [A, B, C, \alpha, a_0].$$

As a general form, these five parameters can be dependent on or independent of the flow rate and/or the current input depending on the selected method of parameter identification. However, in common, at least one of these parameters should be dependent on the current input since the current input applied, as one of the independent variables is not yet accommodated in the generalized form of the model.

In order to identify the values of model parameters, the characteristics of MR valve at frequency excitation of 0.75 Hz are taken as a reference. The identification process of the model parameter is conducted using the gradient descent method through the Parameter Estimation Tool (PET) in MATLAB. The method is used to determine the optimum values of the five different parameters to match the model predictions and the experimental data. Since the curve is unique for different current input, there are also unique sets of parameter values for each curve. The collection of each parameter values for different current input are then retraced to find its trend line. The approximated functions of the trend line will be the empirical function to determine the parameter values with respect to the variation in the current input similarly with the approach demonstrated by Jiang and Christenson [32].

**Table 3** List of approximated function for different parameters

Parameters	Approximated functions
<i>A</i>	$-1.1612i^3 + 1.397i^2 + 0.3613i + 0.0391$
<i>B</i>	$-22.33i^5 + 181.31i^4 - 324.92i^3 + 192.26i^2 + 7.37i + 2.035$
<i>C</i>	$2.268i^3 + 0.6812i^2 + 1.1267i + 0.0683$
$\alpha$	$3.6414i^4 - 9.1188i^3 + 8.032i^2 - 3.247i + 1.2009$
$a_0$	1.0

The approximated function will be specific for each parameter for a bonded range of the current input. The functions are needed so that the model, although case specific, can be used in a more compact form of mathematical functions and more practical to be used in control design process. The approximated functions for each parameter are given in Table 3.

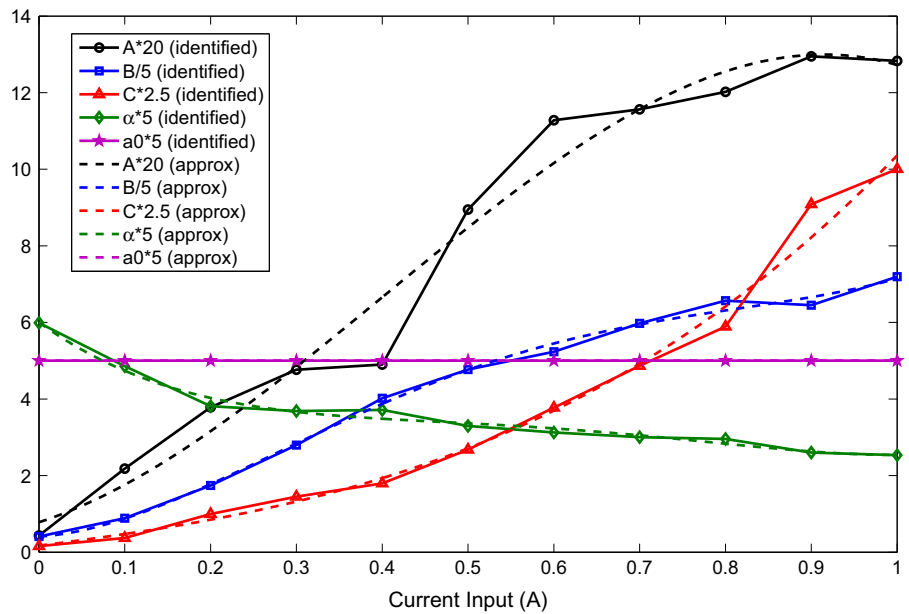
Figure 9 shows the trend comparison of normalized identified and approximated parameters at various current inputs. According to the figure, *A*, *B* and  $\alpha$  tend to increase, *C* tends to decrease and  $a_0$  is intentionally made invariant to the current input. The approximated parameters, as the results from the approximated functions given in Table 3, are also showing similar trends. Although there are some fluctuations, the overall trend of the parameters did not qualitatively change.

### 5 Model performance verification

In this section, the performance of the LuGre-based hysteresis model is evaluated by comparing the model output with the results from polynomial-based hysteresis model for MR valve and the experimental data. The simulation results of both polynomial model and the LuGre model in comparison with the experimental data for frequency excitation of 0.75 Hz at current inputs of 0.3 A, 0.6 A and 0.9 A are shown in Fig. 10a–c, respectively.

Generally, in these figures, the results from both models are in a good agreement with the experimental data, especially in terms of the peak pressure drop value. Though there are some compromises when the curve is reaching the pressure drop of 0 MPa due to the air pocket effect as mentioned in Sect. 3.2, these air pocket effects, unfortunately, failed to be represented in the model and apparently have been tampering the parameter values during the parameter identification

**Fig. 9** Trend comparison of identified and approximated parameters with respect to current input



process. In order to evaluate the accuracy of the model, a specific measurement needs to be taken. In this study, the relative error, which is adopted from [20], is used to measure the level of accuracy of each model and can be expressed in the following equation:

$$RE = \frac{\sum_{i=1}^n |\Delta P_i^{exp} - \Delta P_i^{model}|}{\sum_{i=1}^n |\Delta P_i^{exp}|} \quad (10)$$

where  $n$  is the number of measurement points,  $\Delta P_i^{exp}$  is the experimental data of pressure drop at  $i$ -th point and  $\Delta P_i^{model}$  is the  $i$ -th pressure drop obtained from the model. The comparison of relative error between the polynomial-based nonparametric model and the LuGre-based parametric model is presented in Table 4

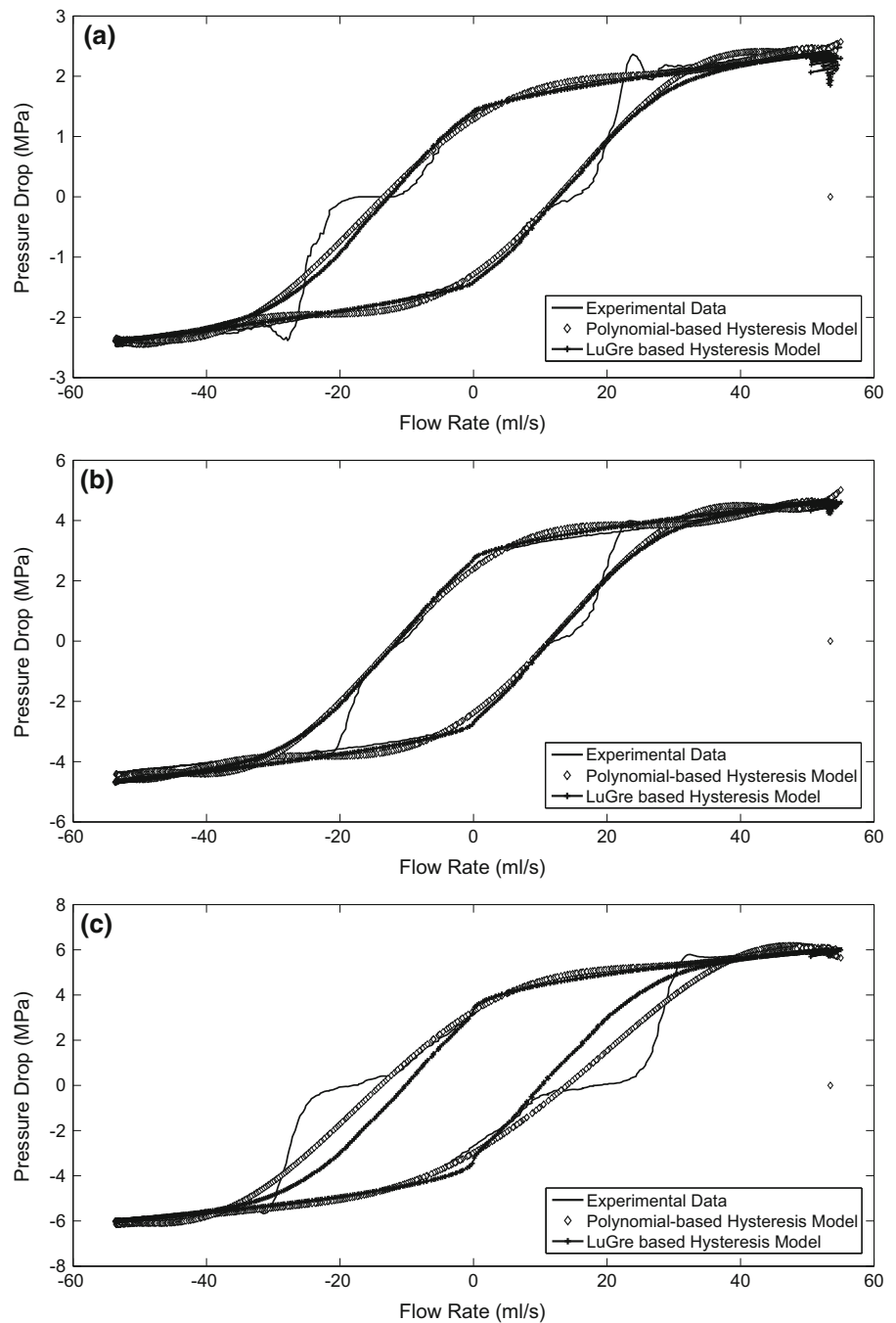
According to Table 4, most of the results from both models are showing relative error <10%, which can be considered good since the results from the model developed by [20] were reported to have even higher relative error (around 15%). In average, the relative error of the polynomial-based hysteresis model is also lower than the relative error of the LuGre-based hysteresis model, which is demonstrating the advantage of the polynomial model in terms of accuracy.

However, the good agreement given in Table 4 is quite obvious since the model output is compared with the measurement data at 0.75 Hz that is used in the parameter identification process. The real performance of the model should be observed at the frequency excitations other than 0.75 Hz. For this reason, the evalua-

tions of the model performance with the experimental data at 0.50 and 1.00 Hz frequency excitations are performed. As a sample case, the comparisons of pressure drop–flow rate characteristics for current input of 1.0 A are shown in Fig. 11. The results in these figures have shown that the deviations are more apparent for both models in the 0.50 and 1.00 Hz frequency excitations. However, the deviations of the polynomial-based hysteresis model are seen much larger than the deviations of the LuGre-based hysteresis model, which are shown by the comparison of relative error in Table 5. These large deviations can be explained by considering that the polynomial equations, at some values, will reach its extreme points. In this case, the extreme points of the pressure drop are visible at the 1.00 Hz frequency excitations, which occurred at the flow rate slightly below  $\pm 55$  ml/s.

According to the model verification results, it can be concluded that the polynomial-based nonparametric model is actually providing better accuracy than the LuGre-based parametric model but only as far as the model inputs are similar to the inputs used in the model development. The LuGre-based parametric model, on the other hand, although cannot compete with the polynomial-based model in terms of accuracy, is shown the capability to show a decent performance and smaller deviations to the measurement data in wider range of model inputs. Additionally, the number of parameters of the LuGre-based parametric

**Fig. 10** Comparison between the test data and the model results for various current input, **a** 0.3 A, **b** 0.6 A, **c** 0.9 A



model is also smaller than that of the polynomial-based nonparametric model so that the parameter identification process is relatively easier. Although it should be noted that the accuracy of the parametric model is not just determined by the model form but also by the identification method of the parameters [31]. The good

agreement between the valve experimental data and the model showed that the model can be used for developing further applications of the MR valve including actuator design and damper design as well as the development of control system for suspension and vibration isolation devices that involves MR fluids flow control.



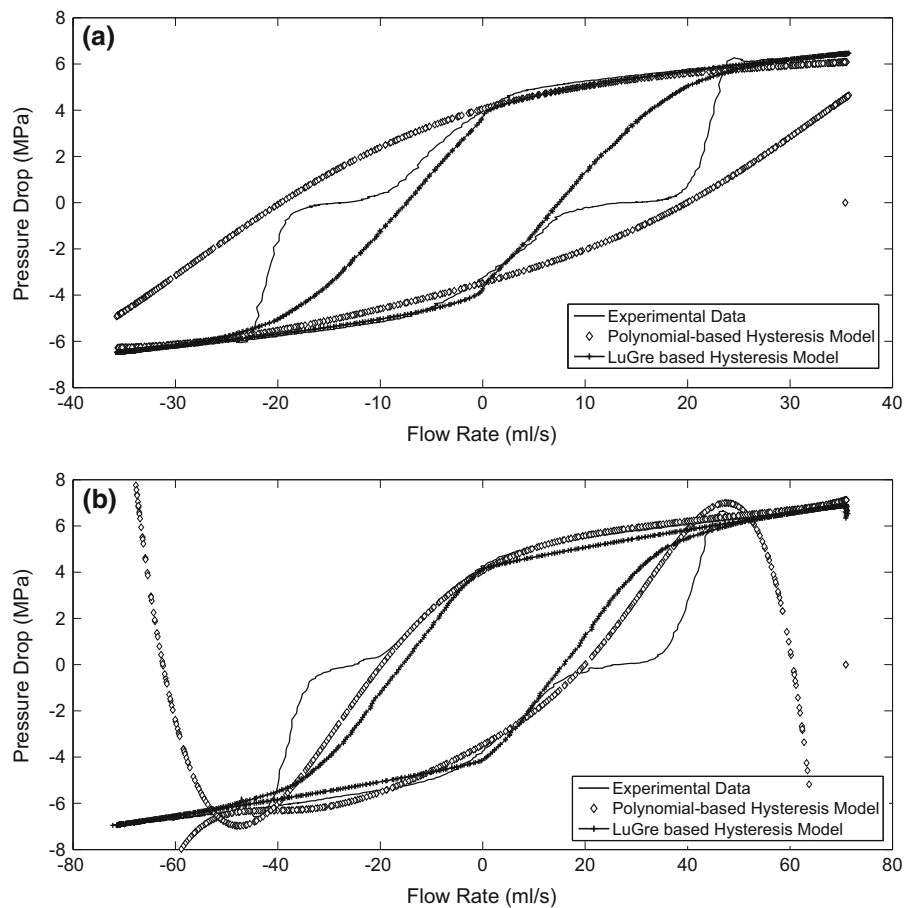
**Table 4** Comparison of relative error at 0.75 Hz frequency excitation

Current input (A)	Relative error	
	Polynomial-based model	LuGre-based model
0.0	0.0813	0.0805
0.1	0.0805	0.1048
0.2	0.0686	0.0566
0.3	0.0609	0.0662
0.4	0.0963	0.1027
0.5	0.0639	0.0522
0.6	0.0641	0.0612
0.7	0.0518	0.0418
0.8	0.0510	0.0556
0.9	0.0644	0.0944
1.0	0.0792	0.1186
Average	0.0693	0.0759

**Table 5** Comparison of relative error at 0.50 and 1.00 Hz frequency excitations

Current Input (A)	Relative error			
	Polynomial-based model		LuGre-based model	
	0.50 Hz	1.00 Hz	0.50 Hz	1.00 Hz
0.0	0.1268	0.5871	0.0767	0.0674
0.1	0.1240	0.5132	0.1053	0.0950
0.2	0.1582	0.5029	0.0685	0.0544
0.3	0.1670	0.6500	0.0894	0.0507
0.4	0.1891	0.8125	0.1274	0.0803
0.5	0.1550	0.9269	0.0603	0.0682
0.6	0.1503	1.0091	0.0669	0.1066
0.7	0.1405	0.9001	0.0614	0.0757
0.8	0.1794	0.6162	0.1098	0.0423
0.9	0.2073	0.3196	0.1424	0.0821
1.0	0.3033	0.8669	0.1427	0.1369
Average	0.1728	0.7004	0.0955	0.0781

**Fig. 11** Comparison between the test data and the model results for current input of 1.0 A at various frequency excitations, **a** 0.50 Hz, **b** 1.00 Hz



## 6 Conclusion

The experimental assessment of the dynamic behavior of a new concept of MR valve with meandering flow path has been demonstrated. The measurement results have shown that the dynamic relationship between the pressure drop and the flow rate of the MR fluid across the MR valve exhibits hysteresis phenomenon which was unable to be described in the steady-state model. In order to model the hysteresis phenomenon, a parametric modeling approach was discussed in this paper. The parametric hysteresis model was developed based on the LuGre friction operator with modification in the model form to reduce the number of parameter involved. The parameter of the LuGre-based parametric hysteresis model was identified with reference to the experimental results of 0.75 Hz excitation frequency. The performance assessment was conducted by comparing the LuGre model output with the polynomial model output in terms of relative error with the experimental results. According to the performance assessment results, both LuGre and polynomial model were showing good agreement with the experimental results with average relative error around 7.6 and 6.9% for LuGre model and polynomial model, respectively. The errors were gradually increased in the excitation frequencies of 0.50 and 1.00 Hz for both models. However, while the average relative error of the LuGre model can be kept <10%, the average relative error of the polynomial model at 0.50 Hz was higher than 15%.

**Acknowledgments** Authors would like to thank Professor Takeshi Mizuno of Saitama University for his valuable comments to the initial draft of this paper. The financial support from the Malaysian Ministry of Higher Education through PRGS Grant No. 4L667 is also acknowledged.

## References

- Hudha, K., Jamaluddin, H., Samin, P.M., Rahman, R.A.: Non-parametric linearised data driven modelling and force tracking control of a magnetorheological damper. *Int. J. Veh. Des.* **46**, 250 (2008)
- Dong, X., Yu, M., Liao, C., Chen, W.: Comparative research on semi-active control strategies for magneto-rheological suspension. *Nonlinear Dyn.* **59**, 433–453 (2009)
- Titurus, B., Lieven, N.: Modeling and analysis of semi-active dampers in periodic working environments. *AIAA J.* **47**, 2404–2416 (2009)
- Wang, D.H., Liao, W.H.: Semi-active suspension systems for railway vehicles using magnetorheological dampers. Part I: system integration and modelling. *Veh. Syst. Dyn.* **47**, 1305–1325 (2009)
- Ubaidillah, U., Hudha, K., Jamaluddin, H.: Simulation and experimental evaluation on a skyhook policy-based fuzzy logic control for semi-active suspension system. *Int. J. Struct. Eng.* **2**, 243–272 (2011)
- Duan, Y.F., Ni, Y.Q., Ko, J.M.: Cable vibration control using magnetorheological dampers. *J. Intell. Mater. Syst. Struct.* **17**, 321–325 (2006)
- Lin, Y.Z., Christenson, R.: Real-time hybrid test validation of a MR damper controlled building with shake table tests. *Adv. Struct. Eng.* **14**, 79–92 (2011)
- Wu, B., Shi, P., Ou, J.: Seismic performance of structures incorporating magnetorheological dampers with pseudo-NEGATIVE STIFFNESS. *Struct. Control Health Monit.* **20**, 405–421 (2013)
- Weber, F., Mašlanka, M.: Precise stiffness and damping emulation with MR dampers and its application to semi-active tuned mass dampers of Wolgograd Bridge. *Smart Mater. Struct.* **23**, 015019 (2014)
- Weber, F., Distl, H.: Amplitude and frequency independent cable damping of Sutong Bridge and Russky Bridge by magnetorheological dampers. *Struct. Control Health Monit.* **22**, 237–254 (2015)
- Imaduddin, F., Mazlan, S.A., Zamzuri, H., Yazid, I.I.M.: Design and performance analysis of a compact magnetorheological valve with multiple annular and radial gaps. *J. Intell. Mater. Syst. Struct.* **26**, 1038–1049 (2015)
- Bhowmik, S., Weber, F., Hogsberg, J.: Experimental calibration of forward and inverse neural networks for rotary type magnetorheological damper. *Struct. Eng. Mech.* **46**, 673–693 (2013)
- Tsang, H.H., Su, R.K.L., Chandler, A.M.: Simplified inverse dynamics models for MR fluid dampers. *Eng. Struct.* **28**, 327–341 (2006)
- Yang, F., Sedaghati, R., Esmailzadeh, E.: Development of LuGre friction model for large-scale magneto-rheological fluid dampers. *J. Intell. Mater. Syst. Struct.* **20**, 923–937 (2009)
- Weber, F., Bhowmik, S., Høgsberg, J.: Extended neural network-based scheme for real-time force tracking with magnetorheological dampers. *Struct. Control Health Monit.* **21**, 225–247 (2014)
- Weber, F.: Robust force tracking control scheme for MR dampers. *Struct. Control Health Monit.* **22**, 1373–1395 (2015)
- Zeinali, M., Mazlan, S.A., Fatah, A.Y.A., Zamzuri, H.: A phenomenological dynamic model of a magnetorheological damper using a neuro-fuzzy system. *Smart Mater. Struct.* **22**, 125013 (2013)
- Snyder, R.A., Kamath, G.M., Wereley, N.M.: Characterization and analysis of magnetorheological damper behavior under sinusoidal loading. *AIAA J.* **39**, 1240–1253 (2001)
- Spaggiari, A., Dragoni, E.: Efficient dynamic modelling and characterization of a magnetorheological damper. *Meccanica* **47**, 2041–2054 (2012)
- Dominguez-Gonzalez, A., Stiharu, I., Sedaghati, R.: Practical hysteresis model for magnetorheological dampers. *J. Intell. Mater. Syst. Struct.* **25**, 967–79 (2014)
- Sakai, C., Ohmori, H., Sano, A.: Modeling of MR damper with hysteresis for adaptive vibration control. In: Proceed-

- ings of 42nd IEEE International Conference on Decision and Control, pp. 3840–3845. IEEE, Maui, Hawaii (2003)
22. Jimenez, R., Alvarez-Icaza, L.: LuGre friction model for a magnetorheological damper. *Struct. Control Health Monit.* **12**, 91–116 (2005)
  23. Ikhrouane, F., Rodellar, J.: On the hysteretic Bouc–Wen model part I: forced limit cycle characterization. *Nonlinear Dyn.* **42**, 63–78 (2005)
  24. Ikhrouane, F., Rodellar, J.: On the hysteretic Bouc–Wen model part II: robust parametric identification. *Nonlinear Dyn.* **42**, 79–95 (2005)
  25. Ikhrouane, F., Hurtado, J.E., Rodellar, J.: Variation of the hysteresis loop with the Bouc–Wen model parameters. *Nonlinear Dyn.* **48**, 361–380 (2007)
  26. Kwok, N.M., Ha, Q.P., Nguyen, T.H., Li, J., Samali, B.: A novel hysteretic model for magnetorheological fluid dampers and parameter identification using particle swarm optimization. *Sens. Actuators A Phys.* **132**, 441–451 (2006)
  27. Kwok, N.M., Ha, Q.P., Nguyen, M.T., Li, J., Samali, B.: Bouc–Wen model parameter identification for a MR fluid damper using computationally efficient GA. *ISA Trans.* **46**, 167–179 (2007)
  28. Ikhrouane, F., Dyke, S.J.: Modeling and identification of a shear mode magnetorheological damper. *Smart Mater. Struct.* **16**, 605–616 (2007)
  29. Rochdi, Y., Giri, F., Ikhrouane, F., Chaoui, F.Z., Rodellar, J.: Parametric identification of nonlinear hysteretic systems. *Nonlinear Dyn.* **58**, 393–404 (2009)
  30. Sahin, I., Engin, T., Çesmecci, S.: Comparison of some existing parametric models for magnetorheological fluid dampers. *Smart Mater. Struct.* **19**, 35012 (2010)
  31. Wang, D.H., Liao, W.H.: Magnetorheological fluid dampers: a review of parametric modelling. *Smart Mater. Struct.* **20**, 023001 (2011)
  32. Jiang, Z., Christenson, R.E.: A fully dynamic magnetorheological fluid damper model. *Smart Mater. Struct.* **21**, 065002 (2012)
  33. Zhang, X.-C., Xu, Z.-D.: Testing and modeling of a CLEMR damper and its application in structural vibration reduction. *Nonlinear Dyn.* **70**, 1575–1588 (2012)
  34. Xia, P.-Q.: An inverse model of MR damper using optimal neural network and system identification. *J. Sound Vib.* **266**, 1009–1023 (2003)
  35. Wang, D.H., Liao, W.H.: Modeling and control of magnetorheological fluid dampers using neural networks. *Smart Mater. Struct.* **14**, 111–126 (2005)
  36. Boada, M.J.L., Calvo, J.A., Boada, B.L., Díaz, V.: Modeling of a magnetorheological damper by recursive lazy learning. *Int. J. Non Linear Mech.* **46**, 479–485 (2011)
  37. Tudón-Martínez, J.C., Lozoya-Santos, J.J., Morales-Menendez, R., Ramírez-Mendoza, R.A.: An experimental artificial-neural-network-based modeling of magnetorheological fluid dampers. *Smart Mater. Struct.* **21**, 085007 (2012)
  38. Choi, S.-B., Lee, S.-K., Park, Y.-P.: A hysteresis model for the field-dependent damping force of a magnetorheological damper. *J. Sound Vib.* **245**, 375–383 (2001)
  39. Ubaidillah, U., Hudha, K., Kadir, F.A.: Modelling, characterisation and force tracking control of a magnetorheological damper under harmonic excitation. *Int. J. Model. Identif. Control* **13**, 9–21 (2011)
  40. Yoo, J.-H., Wereley, N.M.: Design of a high-efficiency magnetorheological valve. *J. Intell. Mater. Syst. Struct.* **13**, 679–685 (2002)
  41. Wang, X., Gordaninejad, F., Hitchcock, G.H., Bangrakulur, K., Fuchs, A., Elkins, J., Evrensel, C.A., Dogruer, U., Ruan, S., Siino, M., Kerns, M.Q.: A new modular magnetorheological fluid valve for large-scale seismic applications. In: Wang, K.-W. (ed.) *Proceedings SPIE 5386*, vol. 5386, pp. 226–237. SPIE, Bellingham, WA (2004)
  42. Ai, H.X., Wang, D.H., Liao, W.H.: Design and modeling of a magnetorheological valve with both annular and radial flow paths. *J. Intell. Mater. Syst. Struct.* **17**, 327–334 (2006)
  43. Salloom, M.Y., Samad, Z.: Design and modeling magnetorheological directional control valve. *J. Intell. Mater. Syst. Struct.* **23**, 155–167 (2011)
  44. Imaduddin, F., Mazlan, S.A., Zamzuri, H., Rahman, M.A.A.: Bypass rotary magnetorheological damper for automotive applications. *Appl. Mech. Mater.* **663**, 685–689 (2014)
  45. Abd Fatah, A.Y., Mazlan, S.A., Koga, T., Zamzuri, H., Zeinali, M., Imaduddin, F.: A review of design and modeling of magnetorheological valve. *Int. J. Mod. Phys. B* **29**, 1530004 (2015)
  46. Imaduddin, F., Mazlan, S.A., Rahman, M.A.A., Zamzuri, H., Ubaidillah, U., Ichwan, B.: A high performance magnetorheological valve with a meandering flow path. *Smart Mater. Struct.* **23**, 065017 (2014)
  47. Yoo, J.-H., Sirohi, J., Wereley, N.M.: A magnetorheological piezohydraulic actuator. *J. Intell. Mater. Syst. Struct.* **16**, 945–953 (2005)
  48. Yoshida, K., Soga, T., Kawachi, M., Edamura, K., Yokota, S.: Magneto-rheological valve-integrated cylinder and its application. *Proc. Inst. Mech. Eng. Part I J. Syst. Control Eng.* **224**, 31–40 (2010)
  49. Imaduddin, F., Mazlan, S.A., Zamzuri, H.: A design and modelling review of rotary magnetorheological damper. *Mater. Des.* **51**, 575–591 (2013)
  50. Lord Corp: *Lord Product Selector Guide: Lord Magneto-Rheological Fluids*, vol. 130, pp. 1–2 (2008)
  51. Yazid, I.I.M., Mazlan, S.A., Kikuchi, T., Zamzuri, H., Imaduddin, F.: Magnetic circuit optimization in designing Magnetorheological damper. *Smart Struct. Syst.* **14**, 869–881 (2014)
  52. Ubaidillah, U., Imaduddin, F., Nizam, M., Mazlan, S.A.: Response of a magnetorheological brake under inertial loads. *Int. J. Electr. Eng. Inf.* **7**, 308–322 (2015)
  53. Tan, K.P., Stanway, R., Bullough, W.: Braking responses of inertia/load by using an electro-rheological (ER) brake. *Mechatronics* **17**, 277–289 (2007)
  54. Karakoc, K., Park, E.J., Suleman, A.: Design considerations for an automotive magnetorheological brake. *Mechatronics* **18**, 434–447 (2008)
  55. Lord Corp: *Lord Technical Data: MRF-132DG Magneto-Rheological Fluid*, vol. 15, pp. 1–2 (2011)
  56. Yoshida, K., Takahashi, H., Yokota, S., Kawachi, M., Edamura, K.: Bellows-driven motion control system using a magneto-rheological fluid. In: *Proceedings of JFPS International Symposium Fluid Power*, pp. 403–408 (2002)

57. Wang, D.H., Ai, H.X., Liao, W.H.: A magnetorheological valve with both annular and radial fluid flow resistance gaps. *Smart Mater. Struct.* **18**, 115001 (2009)
58. Salloom, M.Y., Samad, Z.: Experimental test of magnetorheological directional control valve. *Adv. Mater. Res.* **383–390**, 5409–5413 (2011)
59. Li, W.H., Yao, G.Z., Chen, G., Yeo, S.H., Yap, F.F.: Testing and steady state modeling of a linear MR damper under sinusoidal loading. *Smart Mater. Struct.* **9**, 95–102 (2000)
60. Yang, G.: Large-scale magnetorheological fluid damper for vibration mitigation: modeling, testing and control. PhD Dissertation, University of Notre Dame (2001)
61. Zhang, H.H., Liao, C.R., Yu, M., Huang, S.L.: A study of an inner bypass magneto-rheological damper with magnetic bias. *Smart Mater. Struct.* **16**, N40–N46 (2007)
62. Yun, Y.-W., Lee, S.-M., Park, M.-K.: A study on the efficiency improvement of a passive oil damper using an MR accumulator. *J. Mech. Sci. Technol.* **24**, 2297–2305 (2010)
63. Cook, E., Hu, W., Wereley, N.M.: Magnetorheological bypass damper exploiting flow through a porous channel. *J. Intell. Mater. Syst. Struct.* **18**, 1197–1203 (2007)
64. Canudas de Wit, C., Olsson, H., Astrom, K.J., Lischinsky, P.: A new model for control of systems with friction. *IEEE Trans. Autom. Control* **40**, 419–425 (1995)
65. Lischinsky, P., Canudas-de-Wit, C., Morel, G.: Friction compensation for an industrial hydraulic robot. *IEEE Control Syst. Mag.* **19**, 25–32 (1999)
66. Yang, G., Spencer, B.F., Jung, H., Carlson, J.D.: Dynamic modeling of large-scale magnetorheological damper systems for civil engineering applications. *J. Eng. Mech.* **130**, 1107–1114 (2004)
67. Weber, F.: Bouc–Wen model-based real-time force tracking scheme for MR dampers. *Smart Mater. Struct.* **22**, 045012 (2013)